The Equatorial and Polar Limb-Darkening of Venus in the 8–20 μm Region[1]

DAVID J. DINER[2]

Division of Geological and Planetary Sciences, California Institute of Technology, Pasadena 91125

(Manuscript received 20 June 1978, in final form 6 September 1978)

ABSTRACT

The spectral dependence of limb-darkening of Venus in the 8–20 μm region has been measured for both the equatorial and polar directions. It is shown that the magnitude and spectral variation of the polar darkening are, in general, greater than the equatorial darkening. The equatorial darkening, in fact, appears to be nearly spectrally invariant in this wavelength region, at least for the portion of the disk covered by the observations. The magnitude of the equatorial darkening is consistent with a temperature lapse rate of roughly 3 K km^{-1}, assuming a model in which aerosol is distributed exponentially and mixed homogeneously with atmospheric gas.

1. Introduction

Infrared limb-darkening measurements provide a useful tool for studying the optical and thermal properties of a planetary atmosphere. The spectral dependence of limb-darkening gives some insight into the influence of wavelength-dependent properties (e.g., extinction coefficients) on the observed intensity distribution. This paper presents a study of the limb-darkening of Venus in the 8–20 μm region and contrasts the spectral behavior of the equatorial and polar center-to-limb brightness variations.

The formal relation between intensity as a function of viewing angle cosine μ and wavelength λ is given by the integral expression of the equation of transfer for a semi-infinite atmosphere

$$B_\lambda(\mu)=\int_0^\infty J_\lambda(\tau_\lambda)\exp(-\tau_\lambda/\mu)d\tau_\lambda/\mu, \qquad (1)$$

where $J_\lambda(\tau_\lambda)$ is the radiation source function at optical depth τ_λ. Thus, $B_\lambda(\mu)$, which is the measured quantity, is related to the Laplace transform of the function J_λ. In those instances in which scattering is negligible, the source function is purely thermal, i.e., $J_\lambda(\tau_\lambda)=\mathcal{B}_\lambda(T)$, where $\mathcal{B}$ is the Planck blackbody function, which depends only on the ambient temperature and the wavelength of interest. Solution of Eq. (1) for $J_\lambda(\tau_\lambda)=\mathcal{B}_\lambda(T)$ translates readily into $T(\tau_\lambda)$, i.e., temperature as a function of optical depth for a given wavelength. If further information is available which provides temperature as a function of height, $T(z)$, then $\tau_\lambda(z)$ may be obtained. Given data regarding chemical composition of the opacity sources, and since τ_λ is defined as

$$\tau_\lambda(z)=\int_z^\infty k_\lambda(z)N(z)dz, \qquad (2)$$

where k_λ is the extinction cross section and N the number density, then one can obtain information regarding extinction and density as a function of height in the atmosphere.

Direct inversion of (1) requires knowledge of $B_\lambda(\mu)$ over the entire range of μ, which is a difficult state to achieve observationally. Nevertheless, the information contained in limb-darkening curves for values of $\mu > 0.5$, the observational limit in this study, can be used to evaluate atmospheric models. It will be shown that for these geometries the equatorial limb-darkening in the 8–20 μm region is independent of wavelength. A simple atmospheric model will be considered in an effort to demonstrate the conditions under which this observation may be reproduced. Finally, it will be demonstrated that the spectral dependence of the polar limb-darkening is significantly different from that along the equator.

2. Data

The data used in this paper consist of digital images obtained during the 1975 Venus apparition at the Hale 200-inch telescope. The observational hardware, imaging technique and data processing methods have been discussed in Diner and Westphal (1978a), and the reader is referred to this source. In addition to the

[1] Contribution No. 3035, Division of Geological and Planetary Sciences, California Institute of Technology.

[2] Present affiliation: Earth and Space Sciences Division, Jet Propulsion Laboratory, Pasadena, CA 91103.

0022-4928/78/2356-2361$05.00

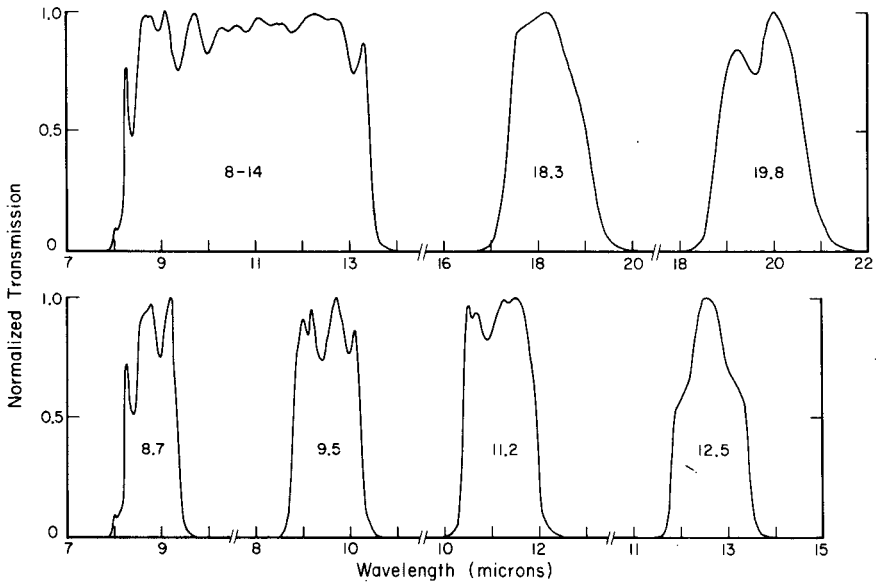

FIG. 1. Normalized spectral transmission characteristics of the filters used in this study. These functions do not include the effects of variable transmission of the telluric atmosphere in the 8–20 μm region.

broadband 8–14 μm channel discussed in that paper, six narrowband channels were used as well. These will be referenced according to their central wavelengths as follows: 8.7, 9.5, 11.2, 12.5, 18.3 and 19.8 μm. Fig. 1 shows the spectral characteristics of each of the filters used. A summary of the observations relevant to the data used in this paper is presented in Table 1.

In another paper (Diner and Westphal, 1978b), we discussed the separation of mean equatorial limb-darkening curves from diurnal brightness variations. These curves are expressed as third-order polynomials, i.e.,

$$\frac{B(\mu)}{B(1)}=1+a(\mu-1)+b(\mu^2-1)+c(\mu^3-1), \qquad (3)$$

where $B(1)$ is the intensity of the center of the disk and a, b and c are given in Table 2 for the narrowband 8.7, 9.5, 11.2, 12.5, 18.3 and 19.8 μm channels as well as for the broadband 8–14 μm channel. Most of the data points in these narrowband channels are from images obtained after inferior conjunction, when the atmosphere is fairly symmetric east–west along the equator. Thus, the limb-darkening is not strongly influenced by the day–night asymmetry in the vicinity of the evening terminator (Diner and Westphal, 1978b).

The polar limb-darkening data are taken from images obtained on UT 26 September 1975 and UT 22 October 1975, the dates upon which the most complete spectral coverage was obtained. The region around the North Pole contained an infrared polar anomaly similar to that observed by Murray *et al.* (1963) and Diner *et al.* (1976) on these dates, whereas the South Pole was more uniform in appearance. Therefore, only the darkening between the disk center and South Pole will be considered in this paper. The mean polar limb-darkening data were fitted by polynomials of the form shown in (3). The coefficients a, b and c are presented in Table 3.

Since no absolute photometric calibrations of the data were obtained, it will be necessary to adopt some value of absolute brightness temperature for the disk center. The value of 235 K will be chosen, consistent with the results of the Venera 9 and 10 and Mariner 10 infrared radiometer measurements (Ksanfomality, 1976; Chase *et al.*, 1974; Taylor, 1975). This value implies that unit optical depth occurs in the 10–50 mb region, assuming the Mariner 5 and 10 radio occultation profiles (Fjeldbo *et al.*, 1971; Howard *et al.*, 1974; Nicholson and Muhleman, 1978). There is a fair amount of evidence that concentrated solutions of H_2SO_4 comprise the major constituent of the clouds at these levels (Hansen and Hovenier, 1974; Young, 1973; Sill, 1972; Pollack *et al.*, 1974; Martonchik, 1974), and that these clouds are poor infrared scatterers such that the source function may be approximated by the Planck blackbody function (Samuelson *et al.*, 1975). In this case, the relation between intensity contrast and brightness temperature difference is given by

$$\frac{\Delta B_\lambda}{B_\lambda}\approx\frac{hc}{\lambda kT_\lambda}\frac{\Delta T_\lambda}{T_\lambda}, \qquad (4)$$

where h is Planck's constant, k Boltzmann's constant and c the speed of light. The following discussion is concerned with the derivation of relative temperature contrasts, rather than absolute values. Thus, the choice of 235 K as the absolute brightness temperature is not too critical and it may be seen from Eq. (4) that the

TABLE 1. Observational log.

Date (UT)	Venus semi-diameter (arcsec)	Venus phase angle (deg)
4 July 1975	14.4	102
5 July 1975	14.6	103
20 July 1975	18.3	116
1 August 1975	22.2	130
26 September 1975	21.6	125
22 October 1975	14.8	100
15 November 1975	11.2	84

use of a value of 10 K higher or lower will not significantly affect the conclusions. Furthermore, although the use of a constant value throughout the 8–14 and 18–20 μm regions is not strictly consistent with the spectral dependence of brightness temperature at these wavelengths (Gillett *et al.*, 1968; Samuelson *et al.*, 1975; Aumann and Orton, 1978), the fact that only relative temperature variations are to be considered renders this a useful, as well as valid approximation.

3. Equatorial limb-darkening

A convenient parameterization of the limb-darkening is the brightness temperature difference between the disk center and the point where $\mu=0.5$, i.e., $T_\lambda(1)-T_\lambda(0.5)$. Using the limb-darkening coefficients in Table 2 to calculate $[B_\lambda(1)-B_\lambda(0.5)]/B_\lambda(1)$, and letting $T_\lambda=235$ K, one can calculate $T_\lambda(1)-T_\lambda(0.5)$ for each wavelength channel. These values are shown in Table 4. Note that this parameter is nearly independent of wavelength, with an average value of about 10.6 K. This result is consistent with any cloud model in which the absorption and scattering properties are wavelength independent. Photometric and spectroscopic measurements of Venus brightness temperature in the 8–20 μm region (Gillett *et al.*, 1968; Samuelson *et al.*, 1975; Aumann and Orton, 1978) and laboratory measurements of the optical properties of H_2SO_4 solutions (Palmer and Williams, 1975) indicate, however, that the Venus clouds are not grey, such that this simple class of models can be ruled out. On the other hand, a cloud model in which 1) the number density of the absorbing aerosol falls off exponentially with altitude and 2) the particle scale height and temperature lapse rate are constant over the range of altitudes sensed in the different wavelength channels also predicts wavelength independent limb-darkening, even though the extinction cross section k_λ may not be spectrally invariant. The following discussion is a demonstration of the validity of this assertion. The implications of this model with respect to scale height and lapse rate are also presented, and a comparison is made with the results of spacecraft radio occultation experiments.

In setting up the model, an exponential distribution of the absorbing aerosol is assumed. The dependence of particle number density N on altitude z may be written $N=N_0\exp[-(z-z_0)/H]$, where N_0 is the particle number density at an altitude z_0 which is below the levels sensed in the infrared and H is the aerosol scale height. Assuming that k_λ and H do not vary with altitude, then from Eq. (2) it follows that

$$\tau_\lambda(z)=Hk_\lambda N_0\exp[-(z-z_0)/H. \tag{5}$$

The atmospheric transmission $\mathcal{T}_\lambda$ above a given altitude z is given by

$$\mathcal{T}_\lambda(z,\mu)=\exp[-\tau_\lambda(z)/\mu]. \tag{6}$$

Neglecting scattering, it follows from Eq. (1) that

$$B_\lambda(\mu)=\int_0^\infty \mathcal{B}_\lambda(z)K_\lambda(z,\mu)dz, \tag{7}$$

TABLE 2. Infrared equatorial limb-darkening parameters for the model $B(\mu)/B(1)=1+a(\mu-1)+b(\mu^2-1)+c(\mu^3-1)$. The model is reliable for $\mu\geq 0.5$ and the uncertainty in $B(\mu)/B(1)$ is approximately ± 0.01 in the 8–14 μm region and ± 0.02 in the 18–20 μm region.

λ (μm)	a	b	c
8.7	0.609	0.410	−0.369
9.5	2.259	−1.770	0.556
11.2	1.516	−0.899	0.163
12.5	1.436	−0.849	0.143
8–14	0.875	−0.129	−0.119
18.3	1.320	−0.709	0.040
19.8	3.263	−3.485	1.307

TABLE 3. As in Table 2 for polar darkening. Only South Pole data were used, as discussed in the text.

λ (μm)	a	b	c
8.7	0.406	0.044	−0.016
9.5	2.165	−2.143	0.892
11.2	0.971	0.102	−0.236
12.5	0.592	0.822	−0.638
8–14	−0.474	1.909	−1.015
18.3	1.570	−1.445	0.595
19.8	0.808	0.002	−0.127

TABLE 4. Equatorial center-to-limb brightness temperature differences (K).

λ (μm)	$[T_\lambda(1)-T_\lambda(0.5)]$
8.7	9.7±0.4
9.5	10.6±0.4
11.2	9.9±0.4
12.5	10.1±0.5
8–14	10.1±0.4
18.3	11.2±1.4
19.8	12.1±1.6

where $K_\lambda(z,\mu)=d\mathcal{T}_\lambda/dz$ and is called the radiative transfer weighting function. Eq. (7) implies that the measured intensity at a given viewing angle is a weighted average of brightness of each level in the atmosphere. In this model, the contribution of $\mathcal{B}_\lambda(z)K_\lambda(z,\mu)$ becomes negligible at a certain altitude and depth and thus the integration in (7) can be finitely bounded. Combining Eqs. (5) and (6), it is seen that

$$K_\lambda(z,\mu)=\exp\left[\frac{-Hk_\lambda N_0}{\mu}\exp[-(z-z_0)/H]\right]^{\frac{k_\lambda N_0}{\mu}} \times\exp[-(z-z_0)/H]. \quad (8)$$

This function has a local maximum such that certain levels will be the most significant contributors to the observed intensity.

The model atmosphere is broken into horizontal layers of 0.5 km vertical thickness and each layer is assumed to be isothermal over its extent. $\mathcal{B}_\lambda$ for a particular layer and spectral channel is calculated from

$$\mathcal{B}_\lambda(z)=\sum_{j=1}^{n}\frac{2hc^2}{\lambda_j^5}\frac{f_j(\lambda_j)}{\exp[hc/(\lambda_j kT)]-1}, \quad (9)$$

where $f_j(\lambda_j)$ is the normalized filter transmission function for a particular channel evaluated at n discrete points in the bandpass. $K_\lambda(z,\mu)$ is calculated from Eq. (8), and Eq. (7) is numerically integrated to yield $B_\lambda(\mu)$. The temperature at the cloud base, $T_0=T(z_0)$, is arbitrarily fixed at 270 K and the lapse rate $\Gamma=-dT/dz$ is assumed constant such that $T(z)=T_0-\Gamma(z-z_0)$.

The essential characteristics of the model are brought to light by using a simplifying approximation in which it is assumed that the observed radiation emanates from a single "effective" level of emission, rather than being a weighted sum of contributions from an extended vertical region. In other words, this single-level approximation defines $B_\lambda(\mu)=\mathcal{B}_\lambda[z'(\mu)]$, where z' is the "effective" altitude at which the blackbody intensity corresponding to the ambient temperature at z' is equal to the observed brightness. Letting τ_λ^* denote the constant slant optical path length between the level $z'(\mu)$ and the observer, and letting τ_λ' equal the vertical optical depth above z', then it follows that

$$\tau_\lambda'=\mu\tau_\lambda^*. \quad (10)$$

Combining Eqs. (5) and (10), one obtains

$$\tau_\lambda^*=(Hk_\lambda N_0/\mu)\exp[-(z'-z_0)/H]=\text{constant}. \quad (11)$$

Solving this equation for the dependence of z' on μ, and remembering that $T'=T_0-\Gamma(z'-z_0)$, then it follows from the single-level approximation that the observed brightness temperature distribution will be given by

$$T_\lambda(\mu)=T_0-\Gamma H\ln(Hk_\lambda N_0/\mu\tau_\lambda^*). \quad (12)$$

TABLE 5. Comparison of 8.7 μm brightness temperatures (K) calculated from integration of the equation of transfer and from the single-level approximation in which radiation is assumed to emanate from the $\tau_\lambda^*=0.73$ level only. The cloud model parameters are $k_\lambda N_0=1.5\times10^{-5}$ cm^{-1}, $H=4.5$ km, $\Gamma=3.3$ K km^{-1}, $T_0=270$ K.

μ	$T_{\text{rad. trans.}}$	$T_{\text{approx.}}$
1.0	234.9	235.1
0.9	233.4	233.5
0.8	231.7	231.7
0.7	229.8	229.7
0.6	227.6	227.4
0.5	225.0	224.7

In order to make use of this approximation, it will be necessary to show that it yields limb-darkening profiles similar to those obtained by using the actual form for $K_\lambda(z,\mu)$ and integrating Eq. (7). Table 5 demonstrates the validity of this single-level approximation for the 8.7 μm channel, and presents the results obtained by converting $B_\lambda(\mu)$ in (7) to equivalent brightness temperatures compared to the results obtained by using the single-level approximation. The parameters were chosen for this example so as to yield a disk center temperature of $\sim$235 K and a center-to-limb brightness temperature difference consistent with the observations. The following values were used: $k_\lambda N_0=1.5\times10^{-5}$ cm^{-1}, $H=4.5$ km, $\Gamma=3.3$ K km^{-1}, $T_0=270$ K, and the agreement shown in Table 5 was obtained by letting $\tau_\lambda^*=0.73$.

Making use of the single-level approximation, it follows from Eq. (12) that the difference in brightness temperature between the center of the disk and the location where $\mu=0.5$ is given by

$$T_\lambda(1)-T_\lambda(0.5)=\Gamma H\ln 2. \quad (13)$$

This equation implies that the observational data are sensitive to the product of Γ and H, and predicts $T_\lambda(1)-T_\lambda(0.5)$ to be independent of wavelength, in agreement with the observations shown in Table 4. Adopting a value of 4.5 km for the scale height H, which is roughly the atmospheric scale height implied by the Mariner 5 and 10 radio occultation experiments (Fjeldbo *et al.*, 1971; Howard *et al.*, 1974; Nicholson and Muhleman, 1978), or in other words, assuming that the aerosol and gas are homogeneously mixed, the average value of $T_\lambda(1)-T_\lambda(0.5)=10.6$ K translates into a lapse rate Γ of slightly greater than 3 K km^{-1}. This number falls between the values of 2.5 and 4 K km^{-1} determined from the two Mariner radio occultation experiments. On the other hand, if a value of 2 km is chosen for the aerosol scale height, which is closer to the value determined from Mariner 10 limb photographs (O'Leary, 1975), the infrared observations imply a lapse rate of nearly 8 K km^{-1}. However, the limb photographs are sensitive to levels where the pressure is a few millibars, and therefore roughly 10 km above the regions to which the infrared measure-

TABLE 6. Polar center-to-limb brightness temperature differences at the South Pole (K).

λ (μm)	$[T_\lambda(1)-T_\lambda(0.5)]$
8.7	7.4±0.4
9.5	9.3±0.4
11.2	15.2±0.4
12.5	17.0±0.5
8–14	12.9±0.4
18.3	15.6±1.4
19.8	22.4±1.6

ments are sensitive. Thus, if an exponentially distributed haze is a reasonable approximation to the Venus cloud structure in the 10–50 mb region, then the limb-darkening and radio occultation measurements are mutually consistent with a model in which the aerosol/gas abundance ratio is independent of altitude, the scale height is on the order of 4.5 km, and the lapse rate is roughly 3 K km^{-1}.

4. Polar limb-darkening

One of the observations made at 8–14 μm by Murray *et al.* (1963) and Westphal *et al.* (1965) and confirmed by the analysis of Ingersoll and Orton (1974) was enhanced limb-darkening in the polar directions compared with the equatorial center-to-limb variation. Analysis of Mariner 10 ultraviolet images (Schubert *et al.*, 1977) indicates primarily zonal transport in the upper atmosphere, and little net motion in the meridional directions. Thus, one may expect that the meridional insolation variation, in which less energy is deposited in the polar regions relative to the equator, will, in radiative equilibrium, be reflected in enhanced poleward infrared limb-darkening. This picture is complicated by the possibility of significant meridional transport of sensible or latent heat below the UV and IR clouds, and the fact that the 8–14 μm region represents only about one-third of the net infrared emission from Venus. Therefore, information regarding the heat budget of the Venus atmosphere requires greater spectral coverage than is presently available, but the spectral dependence of 8–20 μm polar limb-darkening does contain information relevant to the spatial distribution of opacity sources effective at these wavelengths.

It was shown in the previous section that the temperature difference between the disk center and the location where $\mu=0.5$ on the equator is practically wavelength-independent from 8 to 20 μm. Table 6 shows the parameter $T_\lambda(1)-T_\lambda(0.5)$ for each of the wavelength channels, where in this case $T_\lambda(0.5)$ refers to a point on the polar axis in the Southern Hemisphere. The data are computed using the polynomial fits presented in Table 3. It may be seen in Table 6, in contrast with the results obtained in the last section, that the center-to-limb variation in brightness temperature is strongly wavelength dependent in the polar direction. Note that the temperature contrast at 8.7 μm is lower than that obtained in the equatorial direction; at 9.5 μm it is comparable in magnitude; and at all other wavelengths it is significantly greater. The simplest explanation of this observation is that the optical properties of the atmosphere are latitude and wavelength dependent, i.e., that at 8.7 μm the polar regions are less opaque than the equator, and become more opaque longward of 9.5 μm. This change in opacity therefore enhances or detracts from the basic temperature contrast due to the atmospheric temperature lapse rate. A strong possibility is that the vertical structure of the polar regions differs significantly from the structure in the equatorial regions. Alternatively (or simultaneously), the properties of the individual cloud particles may vary from equator to pole. Particles which are on the order of 20–30 μm in radius would appear more opaque to the longer wavelength IR radiation and thus a greater abundance of such particles in the polar regions relative to the low latitudes might be capable of explaining the observed spectral variation in $T_\lambda(1)-T_\lambda(0.5)$. A comparison of the angular distribution of polarization at visible wavelengths of the equatorial versus polar regions may be one possible method of testing this hypothesis. In particular, an increase in polarization near scattering angles of 90° is diagnostic of an increase in particle size for particles larger than the wavelength (Hansen and Travis, 1974). Spatially resolved data obtained at a phase angle of 77° by Coffeen and Gehrels (1969) and discussed by Kawabata and Hansen (1975) in fact indicate greater polarization in the polar regions compared to the lower latitudes.

5. Conclusion

In addition to spatially resolved limb-darkening measurements of the type presented here, another critical test of atmospheric models is conclusive determination of the spectral variation in absolute brightness temperature from 10 to 20 μm. Recent C-141 airborne observations (Aumann and Orton, 1978) indicate that 20 μm brightness temperatures are roughly equivalent to the 10 μm values. On the other hand, ground-based observations (Kunde *et al.*, 1977) indicate that Venus is roughly 30 K warmer at 20 μm than at 10 μm. Clearly, since the combination of spatially and spectrally resolved observations provides a valuable basis for the development of atmospheric models, resolution of this controversy is vital for a better understanding of not only the spectral nature of IR opacity but the vertical distribution of clouds in Venus' upper atmosphere as well.

Acknowledgments. I am indebted to James Westphal for his advice and support during this observing program. I also thank Andrew Ingersoll, Duane

Muhleman, Glenn Orton and Fredric Taylor for many helpful comments, and am grateful to Brad Bailey, Juan Carrasco, Kevin Jordan and Gary Tuton for assistance with the observations. This research was funded by NASA Grant NGL 05-002-003.

REFERENCES

Aumann, G., and G. S. Orton, 1978: The 12–24 μm spectrum of Venus. Submitted to *Icarus*.

Chase, S. C., E. D. Miner, D. Morrison, G. Münch and G. Neugebauer, 1974: Preliminary infrared radiometry of Venus from Mariner 10. *Science*, **183**, 1291–1292.

Coffeen, D. L., and T. Gehrels, 1969: Wavelength dependence of polarization. XV. Observations of Venus. *Astron. J.*, **74**, 433–445.

Diner, D. J., and J. A. Westphal, 1978a: Correlation of simultaneous ultraviolet (0.36 μm) and infrared (8–14 μm) images of Venus. Submitted to *Icarus*.

——, and ——, 1978b: Phase coverage of Venus during the 1975 apparition: Diurnal variations in equatorial infrared brightness. Submitted to *Icarus*.

——, J. A. Westphal and F. P. Schloerb, 1976: Infrared imaging of Venus: 8–14 micrometers: *Icarus*, **27**, 191–195.

Fjeldbo, G., A. J. Kliore and V. R. Eshleman, 1971: The neutral atmosphere of Venus as studied with Mariner V radio occultation experiments. *Astron. J.*, **76**, 123–140.

Gillett, F. C., F. J. Low and W. A. Stein, 1968: Absolute spectrum of Venus from 2.8 to 14 microns. *J. Atmos. Sci.*, **25**, 594–595.

Hansen, J. E., and J. W. Hovenier, 1974: Interpretation of the polarization of Venus. *J. Atmos. Sci.*, **31**, 1137–1159.

——, and L. D. Travis, 1974: Light scattering in planetary atmospheres. *Space Sci. Rev.*, **16**, 527–610.

Howard, H. T., G. L. Tyler, G. Fjeldbo, A. J. Kliore, G. S. Levy, D. L. Brunn, R. Dickinson, R. E. Edelson, W. L. Martin, R. B. Postal, B. Seidel, T. T. Sesplaukis, D. L. Shirley, C. T. Stelzried, D. N. Sweetnam, A. I. Zygielbaum, P. B. Esposito, J. D. Anderson, I. I. Shapiro, and R. D. Reasenberg, 1974: Venus: Mass, gravity field, atmosphere, and ionosphere as measured by the Mariner 10 dual-frequency radio system. *Science*, **183**, 1297–1301.

Ingersoll, A. P., and G. S. Orton, 1974: Lateral inhomogeneities in the Venus atmosphere: Analysis of thermal infrared maps. *Icarus*, **21**, 121–128.

Kawabata, K., and J. E. Hansen, 1975: Interpretation of the variation of polarization over the disk of Venus. *J. Atmos. Sci.*, **32**, 1133–1139.

Ksanfomality, L. V., 1976: Infrared thermal measurements from the artificial satellites of Venus. Publ. 226, Space Res. Inst., USSR Academy of Sciences.

Kunde, V. G., R. A. Hanel, and L. W. Herath, 1977: High spectral resolution ground-based observations of Venus in the 450 to 1250 cm^{-1} region. *Icarus*, **32**, 210–224.

Martonchik, J. V., 1974: Sulfuric acid cloud interpretation of the infrared spectrum of Venus. *Astrophys. J.*, **193**, 495–501.

Murray, B., R. L. Wildey, and J. A. Westphal, 1963: Infrared photometric mapping of Venus through the 8- to 14-micron atmospheric window. *J. Geophys. Res.*, **68**, 4813–4818.

Nicholson P. D., and D. O. Muhleman, 1978: Independent radio occultation studies of Venus' atmosphere. *Icarus*, **33**, 89–101.

O'Leary, B., 1975: Venus: Vertical structure of stratospheric hazes from Mariner 10 pictures. *J. Atmos. Sci.*, **32**, 1091–1100.

Palmer, K. F., and D. Williams, 1975: Optical constants of sulfuric acid. Applications to the clouds of Venus? *Appl. Opt.*, **14**, 208–219.

Pollack, J. B., E. F. Erickson, F. C. Witteborn, C. Chackerian Jr., A. L. Summers, W. Van Camp, B. J. Baldwin, G. C. Angason and L. J. Caroff, 1974: Aircraft observations of Venus' near-infrared reflection spectrum: Implications for cloud composition. *Icarus*, **23**, 8–26.

Samuelson, R. E., R. A. Hanel, L. W. Herath, V. G. Kunde and W. C. Maguire, 1975: Venus cloud properties: Infrared opacity and mass mixing ratio. *Icarus*, **25**, 49–63.

Schubert, G., C. C. Counselman, III, J. Hansen, S. S. Limaye, G. Pettengill, A. Seiff, I. I. Shapiro, V. E. Suomi, F. Taylor, L. Travis, R. Woo and R. E. Young, 1977: Dynamics, winds, circulation and turbulence in the atmosphere of Venus. *Space Sci. Rev.*, **20**, 357–387.

Sill, G. T., 1972: Sulfuric acid in the Venus clouds. *Comm. Lunar Planet. Lab.*, **171**, 191–198.

Taylor, F. W., 1975: Interpretation of Mariner 10 infrared observations of Venus. *J. Atmos. Sci.*, **32**, 1101–1106.

Westphal, J. A., R. L. Wildey and B. C. Murray, 1965: The 8–14 micron appearance of Venus before the 1964 conjunction. *Astrophys. J.*, **142**, 799–802.

Young, A. T., 1973: Are the clouds of Venus sulfuric acid? *Icarus*, **18**, 564–582.